Conserved rotavirus NSP5 and VP2 domains interact and affect viroplasm

Buttafuoco, Antonino ; Michaelsen, Kevin ; Tobler, Kurt ; Ackermann, Mathias ; Fraefel, Cornel ; Eichwald, Catherine

Abstract: One step of the life cycle common among all rotaviruses (RV) studied so far is the formation of viroplasms, membrane-less cytosolic inclusions providing a microenvironment for early morphogenesis and RNA replication. Viroplasm-like structures (VLS) are simplified viroplasm models consisting of complexes of non-structural protein 5 (NSP5) with either the RV core-shell VP2 or NSP2. We identified and characterized the domains required for NSP5-VP2 interaction and VLS formation. VP2 mutations L124A, V865A, or I878A impaired both NSP5 hyperphosphorylation and NSP5/VP2 VLS formation. Moreover, NSP5-VP2 interaction does not depend on NSP5 hyperphosphorylation. The NSP5 tail region is required for VP2 interaction. Notably, VP2 L124A expression acts as dominant-negative by disrupting the formation of either VLSs or viroplasms and blocking RNA synthesis. <jats:italic>In silico</jats:italic> analyses revealed that VP2 L124, V865, and I878 are conserved among RV A to H species. The detailed knowledge of the protein interaction interface required for viroplasm formation may facilitate the design of broad-spectrum antivirals to block RV replication. <jats:bold>Importance</jats:bold> Alternative treatments to combat rotavirus infection are a requirement for susceptible communities where vaccines cannot be applied. This demand is urgent for newborn infants, immunocompromised patients but also for adults traveling to high-risk regions and even for livestock industry. Aside from structural and physiological divergences among RV species studied until now, all replicate within cytosolic inclusions termed viroplasms. These inclusions are composed of viral and cellular proteins and viral RNA. Viroplasm-like structures (VLS), composed of RV proteins NSP5 with either NSP2 or VP2, are models for investigating viroplasms. In this study, we identified a conserved amino acid in the VP2 protein, L124, necessary for its interaction with NSP5 and the formation of both VLSs and viroplasms. As RV vaccines cover a narrow range of viral strains, the identification of VP2 L124 residue lays the foundations for the design of drugs that specifically block NSP5-VP2 interaction as a broad-spectrum RV antiviral.

DOI: https://doi.org/10.1128/jvi.01965-19

Conserved rotavirus NSP5 and VP2 domains interact and affect viroplasm

Antonino Buttafuoco [a], Kevin Michaelsen [a], Kurt Tobler [a], Mathias Ackermann [a], Cornel Fraefel [a], Catherine Eichwald [a#]

[a] Institute of Virology, University of Zurich, 8057 Zurich, Switzerland.

Running Head: NSP5-VP2 interaction region

Address correspondence to Catherine Eichwald, ceichwald@vetvir.uzh.ch

Word counts for abstract and text are 167 and 7'782, respectively

Abstract. One step of the life cycle common among all rotaviruses (RV) studied so far is the formation of viroplasms, membrane-less cytosolic inclusions providing a microenvironment for early morphogenesis and RNA replication. Viroplasm-like structures (VLS) are simplified viroplasm models consisting of complexes of non-structural protein 5 (NSP5) with either the RV core-shell VP2 or NSP2. We identified and characterized the domains required for NSP5-VP2 interaction and VLS formation. VP2 mutations L124A, V865A, or I878A impaired both NSP5 hyperphosphorylation and NSP5/VP2 VLS formation. Moreover, NSP5-VP2 interaction does not depend on NSP5 hyperphosphorylation. The NSP5 tail region is required for VP2 interaction. Notably, VP2 L124A expression acts as dominant-negative by disrupting the formation of either VLSs or viroplasms and blocking RNA synthesis. *In silico* analyses revealed that VP2 L124, V865, and I878 are conserved among RV A to H species. The detailed knowledge of the protein interaction interface required for viroplasm formation may facilitate the design of broad-spectrum antivirals to block RV replication.

Keywords: NSP5 /protein-interface/ VP2 / rotavirus / viroplasm

Importance. Alternative treatments to combat rotavirus infection are a requirement for susceptible communities where vaccines cannot be applied. This demand is urgent for newborn infants, immunocompromised patients but also for adults traveling to high-risk regions and even for livestock industry. Aside from structural and physiological divergences among RV species studied until now, all replicate within cytosolic inclusions

termed viroplasms. These inclusions are composed of viral and cellular proteins and viral RNA. Viroplasm-like structures (VLS), composed of RV proteins NSP5 with either NSP2 or VP2, are models for investigating viroplasms. In this study, we identified a conserved amino acid in the VP2 protein, L124, necessary for its interaction with NSP5 and the formation of both VLSs and viroplasms. As RV vaccines cover a narrow range of viral strains, the identification of VP2 L124 residue lays the foundations for the design of drugs that specifically block NSP5-VP2 interaction as a broad-spectrum RV antiviral.

Introduction

Rotaviruses (RVs) are dsRNA viruses of the Reoviridae family and are responsible for severe gastroenteritis in infants and young children, killing approx. 128,000 children per year, mainly in developing countries (1). RV virions are organized in three concentric layers surrounding the viral genome. The spike protein VP4 and the glycoprotein VP7 form the outermost layer, while VP6 makes up the intermediate layer. The innermost layer, the core-shell, is composed of 120 copies of VP2, organized in twelve asymmetric decamers (2). Each core-shell encapsidates the eleven segments of the viral genome as well as the replication complexes composed of the RNA-depended RNA polymerase (RdRp) VP1 and the guanylyl-methyltransferase VP3. There is evidence that one replication complex locates beneath each 5-fold axis of the twelve VP2 decamers (2, 3). During virus entry, the external layer is lost, and a transcriptionally active double-layered particle is released into the cytosol (4). The newly released transcripts enable the synthesis of viral proteins necessary for viral replication. Among those proteins, the NTPase/RTPase NSP2 and the phosphoprotein NSP5, together with the structural proteins VP1, VP2, VP3, and VP6, and the non-structural NSP4, constitute the RV viral factories termed viroplasms (5, 6). The viroplasms correspond to membrane-less cytosolic electron-dense inclusions where viral genome transcription and replication, as well as the packaging of the newly synthesized pre-genomic RNA segments into the viral cores, take place. Interestingly, co-expression of the main viroplasm protein NSP5 with either NSP2 or VP2 leads to the formation of cytosolic inclusions named viroplasm-like structures (VLS) that are morphologically similar to viroplasms but unable to yield viral progeny (7-12). VLSs serve as a useful simplified model for studying RV viroplasms

since they share physiological traits with viroplasms, including coalescence and perinuclear condensation (10, 13-15). NSP5 is hyperphosphorylated (16, 17) and O-GlcNAc-glycosylated (18). While the role of NSP5 phosphorylation in RV replication remains obscure, it has been demonstrated that NSP2 or VP2 are required to enhance the hyper-phosphorylation state (19, 20). Moreover, NSP5 is required for viroplasm formation and virus replication, as shown by knockdown experiments using siRNAs (21, 22). NSP5 has a multifunctional role in the RV lifecycle, interacting with NSP6 (12), NSP2 (9), VP1 (23), VP2 (24) and in an unspecific manner with dsRNA (25), which also is consistent with its predicted partially unfolded nature (26-28). NSP5 was recently described as covalently sumoylated (29), suggesting that this modification might be a pre-requirement for the interaction with viral or host components. Taken these studies together, NSP5 can be considered an essential component for RV replication. Likewise, the core-shell protein VP2, besides its structural function protecting the viral genome, is also able to activate and regulate the RdRp VP1 protein (30), permitting genome replication. In TLPs and DLPs, VP2 spontaneously oligomerizes by forming an asymmetric decameric structure with VP2 isoforms A and B that converges in the 5-fold axis, which cannot dissociate (2, 28, 31-33). Each subunit of the decamer is composed of a primary domain of VP2 (residues ~ 100 to 880), forming a thin coma shaped plate, which in turn also divides into three subdomains: apical, central and dimer forming. The N-terminal domain (NTD) (residues ~1 to 100 for type A and ~1 to 80 for type B) is unfolded and localizes in the decamer beneath the 5-fold axis. VP1, VP3, VP6, and NSP2 (2, 34-36), as well as unspecific ssRNA (37), have been mapped to bind to VP2, most of them directly associated to the NTD. However, these viral proteins can also make contact

with the VP2 scaffold region, for example, VP1, which contacts the VP2 region 341-374 (38-40). These interactions are all directly related to the core-shell structure and genome replication and transcription. VP2 is also a main component of the viroplasms, as denoted by immunofluorescence of RV infected cells and its ability to form VLS when co-expressed with NSP5 (7, 10, 41). The VLSs induced by VP2 (hereafter, VLS) are dynamic and able to shift to the perinuclear region by a mechanism that is still under investigation (10). Further evidence indicates that VP2 triggers NSP5 hyperphosphorylation (7). Recently it has been suggested that VP2 may have additional roles at early times post-infection because of its interaction with NSP2, preventing its spontaneous oligomerization and sumoylation, which increases the ability of VP2 to interact with other proteins (10, 29). Therefore, we hypothesized that the interaction of these two proteins to form VLS is an essential step for RV replication.

In this study, we show that specific point mutations in VP2 abrogate VLS formation by disrupting NSP5 binding and phosphorylation. Additionally, we demonstrate that NSP5 requires its 18 C-terminal amino acids to interact with VP2 directly. Importantly, VP2 harboring the point mutation L124A disrupts VLS induced by the expression of NSP5-VP2 and NSP5-NSP2. Similarly, in RV-infected cells, VP2 L124A expression results in a reduced number of infected cells, and viroplasms with aberrant structures and defective in viral RNA synthesis. Altogether, these data provide a mechanistic explanation that a conserved NSP5/VP2 interaction interface is required for efficient RV replication.

Results

VP2 amino acid regions 103-135 and 840-880 are necessary for VLS formation with NSP5. To elucidate the nature of the association between NSP5 and VP2, we assessed the capacity of these two proteins to form viroplasm-like structures when co-expressed in the absence of other rotavirus proteins (7). To this end, and as denoted in Fig 1A, we constructed a series of VP2 mutants by deleting N-terminal and C-terminal regions as well as constructs expressing single regions of the protein based on the published tertiary VP2 structure (42). For the detection of the VP2 deletion mutants, a human influenza virus hemagglutinin (HA) tag was added at the N-terminus. All HA-VP2 deletion mutants were verified by immunoblotting for correct expression and size (data not shown). Next, we performed immunofluorescence analysis of co-transfected cells to assess VLS formation, which was considered positive only when co-localization of both HA-VP2 and NSP5 was observed in cytosolic inclusions. The results, summarized in Fig 1, show that full-length HA-VP2 (fl) was homogeneously distributed in the cytosol of transfected cells (Fig 1B, top row, -NSP5). However, when HA-VP2fl was co-expressed with NSP5 (Fig 1B, top row, +NSP5), it formed cytosolic inclusions that co-localized with NSP5, corresponding to VLSs. In the presence of NSP5, HA-VP2ΔN103 was able to form VLSs, while HA-VP2ΔN135 was not (Fig 1B). The shortest HA-VP2 C-terminal deletion mutant tested (Fig 1B), HA-VP2 ΔC840, was also unable to form VLSs when co-expressed with NSP5, suggesting that the amino acid region 840 to 880 is necessary for VLS formation with NSP5 as well. Of note, none of the constructs that tested positive for VLS formation colocalized with ubiquitin when co-expressed with NSP5 (data not

shown), suggesting that the observed structures correspond to genuine VLS. This data indicates that the amino acid regions from 103-135 and 840-880 of VP2 are necessary for VLSs formation between VP2 and NSP5. As expected, none of the HA-VP2 single regions formed VLSs when co-expressed with NSP5. A summary of the results of all HA-VP2 deletion mutants tested for VLS formation is shown in the right column of Fig 1A.

VP2 amino acids L124, V865, and I878 are required for VLS formation. We next determined the residues in region 103-135 of VP2 (RV simian strain SA11) that are relevant for VLS formation. For this, we first performed primary sequence alignment of all VP2 proteins from species A to H (Fig 2A). This analysis revealed that four amino acid residues are highly conserved among all the aligned VP2 proteins, specifically I106, D112, L124, and I127. To analyze their role in VLS formation, we mutated each of these residues to alanine in HA-VP2ΔN103, which is the minimal HA-VP2 deletion mutant able to form VLS when co-expressed with NSP5. The point mutations I106A, D112A, and I127A (data not shown), as well as the parent construct (HA-VP2ΔN103), supported the formation of VLS together with NSP5 while HA-VP2ΔN103 (L124A) did not. VP2 carrying this point mutation (L124A) was also not able to form VLS with NSP5 when introduced into a full-length untagged VP2 (Fig 2C) while wild type (wt) VP2 and VP2 D112A did (D112A was chosen as a positive control for NSP5-HA-VP2ΔN103 VLS formation (data not shown)).

Similarly, as for the VP2 region 103-135, we aligned the amino acid region 840 to 880 of VP2-SA11 using all the NCBI deposited sequences for VP2. This alignment revealed several conserved amino acids in VP2, including M843, L856, V860, V865,

157 F873, and I878, in RV species A-H (Fig 2B). Interestingly, F850 was highly conserved
158 among RVA, RVC, RVF, and RVD species but absent in RVB, RVG, and RVH species.
159 We mutated each of these residues to alanine in wt VP2 and tested for VLS formation in
160 co-expression with NSP5. As shown in Fig 2C, wt VP2, and VP2 harboring point
161 mutations M843A, F850A, L856A, V860A, and F873A were able to form VLS. In
162 contrast, VP2 harboring a point mutation in residues V865 and I878 was unable to form
163 VLS. In contrast to wt VP2, the mutants VP2 V865A and I878A do not diffuse
164 homogeneously in the cytosol. However, they did not form aggresomes (data not shown),
165 either, suggesting the spontaneous generation of genuine or aberrant core-like structures.
166 All the other point mutations maintained their ability to form VLS. Importantly, as
167 observed in Fig 3A, cognate NSP5(SA11)-VP2(SA11) pairs, as well as unrelated
168 NSP5(OSU)-VP2(SA11), can form VLSs. Meanwhile, VP2L124A impairs VLS either
169 with NSP5 (SA11) or NSP5(OSU). Collectively, our data suggest that L124, V865, and
170 I878 of VP2-SA11 are necessary for VLS formation in the presence of NSP5.

171 **VP2 residues L124, V865, and I878 are required for triggering NSP5**
172 **hyperphosphorylation**. NSP5 is a phosphoprotein that during RV-infection shows a
173 mobility shift on SDS-PAGE corresponding to a hyperphosphorylated pattern (16, 17).
174 However, when NSP5 is expressed in the absence of other viral proteins, it is detected
175 only as a single band (19). Interestingly, it has been described that the co-expression of
176 NSP5 with NSP2 (19) and VP2 (7) triggers the NSP5 hyperphosphorylation pattern. In
177 order to determine which VP2 regions are involved in triggering the NSP5
178 hyperphosphorylation, we analyzed cell extracts co-expressing NSP5 in the presence of
179 VP2 constructs with deletions at the N-terminus (Fig 4A) and C-terminus (Fig 4B). As

shown in Fig 4, wt VP2 and VP2ΔN81 (Fig 4A, lanes 2-3, and Fig 4B, lane 2) triggered NSP5 hyperphosphorylation, while all other VP2 deletion mutants tested did not (Fig 4A lanes 4-7 and Fig 4B lanes 3-7), as the NSP5 pattern was comparable to that when NSP5 is expressed alone (Figs 4A and 4B, lane 1). Similarly, VP2 proteins harboring L124A, V865A, and I878A point mutations (Fig 4C, lanes 3-5, and Fig 3B, lanes 3 and 6) failed to induce NSP5 hyperphosphorylation as well (Fig 4C, lane 2 and Fig 3B lanes 2 and 4). As previously demonstrated (19), the treatment of cellular extracts with lambda-phosphatase confirmed that the NSP5 PAGE mobility-shift corresponds to phosphorylation (Fig 4D). Our results suggest that the VP2 residues involved in VP2-NSP5 VLS formation and in triggering NSP5 hyperphosphorylation are identical.

NSP5 S67D cannot restore VLS formation with VP2 L124A. As previously reported, NSP5 hyperphosphorylation is triggered by phosphorylation on serine 67 when in the presence of NSP2 (19) or VP2 (7), due to a mechanism involving casein kinase I alpha (43, 44). Interestingly, when serine 67 (Fig 4E) is mutated to an aspartic acid, which mimics a phosphorylated serine, NSP5 gets hyperphosphorylated similarly as upon RV infection (44). We, therefore, investigated whether NSP5 S67D would allow VLS formation with the VP2 point mutation L124A. For this, we compared VLS formation of wt NSP5 and NSP5 S67D with wt VP2 (Fig 4F, upper panel) or VP2 L124A (Fig 4F, lower panel). As expected, wt NSP5 or NSP5 S67D form VLS with wt VP2 but not with VP2 L124A. In order to test whether the phosphorylation state of NSP5 S67D was impaired when co-expressed with VP2 L124A (Fig 4G), we inspected the NSP5 hyperphosphorylation patterns of both wt NSP5 and NSP5 S67D when co-expressed with wt VP2 (Fig 4G, lanes 2 and 5) or VP2 L124A (Fig 4G, lanes 3 and 6). Wt NSP5, as

anticipated, had an increased mobility shift in the presence of wt VP2 but not in the presence of VP2 L124A, which showed a pattern comparable to that observed when wt NSP5 is expressed alone. Surprisingly, NSP5 S67D showed a more substantial shift with wt VP2 (Fig 4G, lane 2), while with VP2 L124A, a single NSP5 band was detected, similar to that observed when wt NSP5 had expressed alone (Fig 4G, lane 3). Since VP2 triggered NSP5 hyperphosphorylation, we hypothesized that the hypophosphorylation of NSP5 in the presence of VP2 L124A is impaired because of the lack of interaction between the two proteins. To address this (Fig 4H), we pulled down cellular extracts co-expressing hexahistidine (H_6)-tagged wt NSP5 (H_6-NSP5) or NSP5 S67D (H_6-NSP5/S67D) with wt VP2 or VP2 L124A. The results showed that independent of the NSP5 genotype (wt or S67D), VP2 L124 did not bind NSP5 while wt VP2 did. Collectively, this data suggests that NSP5 and VP2 associate to form VLS independent of the NSP5 phosphorylation state.

VP2 L124 and I878 are necessary to bind NSP5. To determine if VP2 and NSP5 requirements for VLS formation correlate with their ability to associate, we performed a pull-down assay by adding an H_6 tag at the N-terminus of NSP5 (H_6-NSP5) followed by co-expression with wt VP2 or VP2 L124A, VP2 V865A or VP2 I878A point mutations (Fig 5A). As expected, wt VP2 associated with NSP5, as evident by the presence of wt VP2 in the eluted fraction (Figs 5A, lane 3). By contrast, VP2 L124A was not detected in the elution (Fig 5A, lanes 6), suggesting no association to H_6-NSP5. Also, VP2 V865A got eluted from the pull-down assay (Fig 5A, lane 9). Meanwhile, VP2 I878 weakly eluted, suggesting no or weak association to NSP5 (Fig 5A, lane 12). Interestingly, when pulling down H_6-NSP5 with wt VP2, the NSP5 eluted fraction showed a higher mobility

shift in PAGE (Fig 5A, lane 3), which represents the NSP5 hyperphosphorylated fraction. The H_6-NSP5 eluted fraction obtained by co-expression with VP2 L124A showed a unique band that correlated with the unphosphorylated NSP5 isoform.

NSP5 amino acid residues 180-198 are necessary for the association with VP2. It was previously described that the NSP5 tail (T), corresponding to residues 180-198, is needed for its dimerization (9, 12, 44) and to associate with NSP2 (9, 35), NSP6 (12) and VP1 (23). Using a pull-down assay, we tested (Fig 5B and C) the capacity of an H_6-tagged, tail-deleted NSP5 (H_6-NSP5ΔT) to bind to VP2. The results show that H_6-NSP5 can bind VP2 while H_6-NSP5ΔT did not. Likewise, H_6-NSP5Δ1Δ3, an NSP5 deletion mutant known to allow self-dimerization (44), pulled-down VP2 whereas the same NSP5 deletion mutant but without the tail region (H_6-NSP5Δ1Δ3ΔT) did not (Fig 5B and D). Interestingly, H_6-NSP5Δ1Δ3 was neither able to pull down VP2 L124A (Fig 5B and E). To confirm these results, we constructed an H_6-tagged EGFP fused at its C-terminus with the NSP5 tail (H_6-EGFP-T) or region 4 (amino acid residues 134-180; H_6-EGFP-4). The fusion constructs were co-expressed with wt VP2 and pulled-down with nickel resin to detect an association with VP2. As shown in Fig 5F and E, H_6-EGFP-T can bind VP2 while H_6-EGFP and H_6-EGFP-4 cannot. Collectively, these results indicate that the NSP5 tail is required for the association with VP2.

VP2 and NSP5 are protein-protein interaction partners. The next experiment was performed to determine whether VP2 and NSP5 proteins can interact directly. For this, we employed the recently developed tripartite split-GFP association assay (45). As shown in Fig 6A, GFP beta strands 10 and 11 are fused to bait (NSP5 or NSP5-T) and prey (wt

248 VP2 or VP2 point mutations), respectively. The detector fragment GFP1-9OPT is added
249 separately. When protein interaction occurs (i), GFP10 and GFP11 are tethered and
250 spontaneously associate with the GFP 1-9 fragment to form a full-length GFP, which
251 fluoresces green. If the bait and prey do not interact (*ii*) GFP10 and GFP11 are not
252 tethered, and the assembly of GFP10, GFP11, and GFP 1-9 does not occur (45);
253 therefore, no green fluorescence is detected by flow cytometry. As expected, neither
254 GFP10-NSP5 nor GFP11-VP2 produced green fluorescence when expressed together
255 with GFP11 or GFP10, respectively (Fig 6B and data not shown). By contrast, co-
256 expression of GFP10-NSP5 with GFP11-VP2 produced green fluorescent cells showing a
257 direct interaction between wt NSP5 and wt VP2. Consistent with the data of the Fig 5A,
258 co-expression of GFP10-NSP5 with either GFP11-VP2 L124A or GFP11-VP2 I878A did
259 not generate green fluorescent cells, thereby confirming their incapacity to interact. By
260 contrast, GFP10-NSP5, together with GFP11-VP2 V865A, as well as GFP10-(T)NSP5
261 together with GFP11-VP2, produced green fluorescent cells. This data confirmed that the
262 NSP5 tail is necessary for the interaction with VP2. Next, we investigated whether VP2
263 L124A would bind to the wtVP2 and thus perturb its interaction with NSP5. To address
264 this question (Fig 6C), we expressed the protein-protein interaction (PPI) partner GFP10-
265 NSP5 and GFP11-VP2 together with an increasing amount of GFP11-VP2 L124A. As
266 anticipated, the PPI partner NSP5-VP2 yielded a high number of green fluorescent cells
267 that were reduced upon the addition of VP2 L124A in a dose-dependent manner,
268 suggesting a reduction in the binding between NSP5 and wt VP2.

269 **VP2 L124A hinders the formation of VLS(NSP5+HA-VP2) and VLS (NSP5+NSP2).**
270 Since VP2 L124A impedes the direct binding of NSP5 and VP2 (Fig 6), we hypothesized

that increased amounts of VP2 L124A would disrupt VLS(NSP5+HA-VP2). To investigate this possibility, we co-expressed NSP5 and HA-VP2 to permit the formation of VLS(NSP5+HA-VP2). As shown in Fig 1B and data not shown, VLS(NSP5+HA-VP2) can be readily detected as yellow-fluorescent cytosolic inclusions upon staining with anti-NSP5 (red) and anti-HA (green) antibodies. With increasing amounts of wt VP2, the color of the VLS shifted to red (Fig 7A), reflecting competition between wt VP2 and HA-VP2. With increasing amounts of VP2 L124A, the cytosolic inclusions became disrupted (Fig 7B). Using the same approach, we then tested whether overexpression of VP2 L124A hinders VLS(NSP5+NSP2) formation. Co-expression of NSP5 and NSP2 resulted in the formation of VLS(NSP5+NSP2), readily detected as yellow-fluorescent cytosolic inclusions upon staining with anti-NSP5 (red) and anti-NSP2 (green) antibodies; VP2 (anti-VP2, green) was not detected (Fig 7C, upper panel). Upon co-expression of NSP5, NSP2, and wt VP2, all three proteins co-localized in the cytosolic VLS (Fig 8C, middle panel). However, when co-expressing NSP5, NSP2, and VP2 L124A, unstructured VLSs were detected (Fig 7C, lower panel). In support of this result (data not shown), a drastic reduction ($p<0.001$) in the number of cells showing VLS(NSP5+NSP2) is observed in co-expression with VP2 L124A (12.8%) compared to wt VP2 (38.3%). Additionally, 100% of VLS(NSP5+NSP2) formed with wt VP2 showed a globular morphology that is in contrast with the reduced number (36%) of globular structures observed among the VLS (NSP5+NSP2) formed with VP2 L124A (data not shown). Accordingly, VP2 L124A expression blocked the formation of both VLS(NSP5+VP2) and VLS(NSP5+NSP2).

293 **VP2 L124A expression affects viroplasm morphology.** As VLSs are a simplified
294 model to study viroplasms, we interrogated whether overexpression of VP2 L124A could
295 also compromise viroplasms formation. For this purpose, we overexpressed either wt
296 VP2 or VP2 L124A in BSR-T7 cells (Fig 8A) followed by RV-infection and quantified
297 cells showing viroplasms under these two conditions. As shown in Fig 8B, the number of
298 cells with viroplasms was significantly reduced upon co-expression of VP2 L124A
299 compared to cells expressing wt VP2. Interestingly, most viroplasms in cells expressing
300 VP2 L124A presented an atypical filamentous (Fig 8C, frames *i* and *ii*) or diffuse and
301 juxtanuclear polarized (Fig 8C, frames *iii* and *iv*) morphology. In contrast, viroplasms
302 formed in the presence of wt VP2-cells showed a characteristic globular morphology (Fig
303 8C, frames *v* and *vi*). Since viroplasms are composed of several host and viral proteins, as
304 well as ssRNAs and dsRNAs, we investigated if the localization of the viral proteins
305 diverges in viroplasms of cells expressing VP2 L124A. For this purpose, RV infected
306 BSR-T7 cells expressing wt VP2, or VP2 L124A, were stained with specific antibodies
307 detecting viroplasm proteins such as NSP5, VP2, VP6, and NSP3 (Fig 8D and data not
308 shown). As expected, (Fig 8D, left panel and data not shown), the viroplasms formed in
309 the presence of wt VP2 expression exhibit delineated globular structures when detected
310 for the tested proteins. However, in the cells expressing VP2 L124A, the viral protein
311 components of viroplasms, including NSP2 and VP6, showed a diffuse pattern (Fig 8D,
312 right panel, and data not shown). For NSP3 and the capsid proteins (VP6, VP7, and VP4,
313 detected by anti-RV antibody), even amyloid-like structures were observed that
314 surrounded aberrant viroplasm structures. Collectively, our data indicate that viroplasm
315 morphology is sensitive to VP2 L124A expression.

316 **VP2 L124A expression precludes transcription and replication.** Since VP2 L124A
317 expression disrupts viroplasm morphology, we inspected if other functions of viroplasms
318 such as viral transcription and replication are also inhibited. The synthesis of RV (+)
319 ssRNA, as a template for dsRNA generation, is uniquely dependent on RdRp-VP1 (46).
320 We assessed RV transcription by treating RV-infected BSR-T7 cells expressing wt VP2
321 or VP2 L124A at 4 hpi with actinomycin D for 30 min (Fig 9A). Of note, actinomycin D
322 has been shown to not interfere with the RdRp activity of VP1 (47). Then, the cells were
323 fed with BrUTP for 1 h, and the incorporation signal was monitored by
324 immunofluorescence using a fluorescence-labelled anti-BrdU antibody. The viroplasms
325 were stained with an anti-NSP5 antibody. Cells not treated with BrUTP were used as
326 control. As expected (46), cells expressing wt VP2 incorporated BrUTP in viroplasms
327 (Fig 9A, upper row) indicating RV viral transcription, while cells expressing VP2 L124A
328 did not (Fig 9A, lower row). To confirm our result, we stained RV-infected cells
329 expressing wt VP2 or VP2 L124A with an anti-dsRNA antibody (clone J2) that can
330 recognize dsRNA with a size larger than 40 base pairs (48). In non-infected cells (Fig 9B,
331 -RV), punctuated anti-dsRNA signal was found distributed in the whole cytoplasm. Upon
332 RV-infection (Fig 9B, +RV), most of the dsRNA signal localized to viroplasms in both
333 non-transfected and wt VP2 expressing cells. These results are also confirmed by
334 intensity profiles among the signals of both viroplasms and dsRNA (Fig 9C). Such
335 pattern, however, is not repeated in VP2 L124A expressing cells, where none or mild
336 localization of anti-dsRNA signal in viroplasm and no coincidence of these signals in the
337 intensity profile plot was observed (Fig 9C). Thus, our results suggest that RV RNA
338 synthesis is at least inefficient in VP2 L124A cells.

Discussion

In RV viroplasms several processes take place, including viral transcription, packaging of the viral pre-genomic RNA into newly synthesized viral cores and RNA replication, followed by the addition of the second layer of proteins. None of these processes have been directly demonstrated as a whole in the viroplasms, and all the current evidence is based on *in vitro* data, providing models, such as the packaging of the virus genome (49). The fact that rotavirus encodes only a small number of proteins, eleven or twelve (NSP6 is present only in certain RV strains (50-53)), supports the hypothesis that at least some viral proteins have multifunctional roles in the replication cycle. A clear example is VP2, which is well characterized as the RV core-shell encapsidating the viral genome (2, 32, 33, 54, 55), acting as co-factor of RdRp VP1 (28, 30, 39), and anchoring VP6 to form DLPs (34, 55). Aside from its structural functions, VP2 has other roles during the RV life cycle, such as permitting perinuclear motion of viroplasms (10) or being associated with the RV induced cell cycle arrest (56). Another exciting aspect is its role as the main building block for viroplasm formation. In this sense, the co-expression of NSP5 with either NSP2 or VP2 forms VLSs denoting the role of VP2 in viroplasm formation (7, 10, 41). In the present study, we fully characterized the interaction between NSP5 and VP2 proteins and the importance of this interaction for VLS formation. In this context, we identified three amino acids in VP2 of simian RV strain SA11, L124, V865, and I878 that are highly conserved among cognate proteins of all RV species present in the NCBI data bank. As observed in the calculated 3D model for VP2-SA11, V865, and I878 (data not shown) are positioned behind the beta-strand β25 at the VP2 dimerization region(2, 57). Accordingly, these hydrophobic residues,

362 when modified to alanine, can directly abrogate VP2 dimerization and VLS formation,
363 indicating that VP2 dimerization is a requirement for VLS formation, in concomitant
364 association with NSP5. A particular example corresponds to VP2 point mutation V865A
365 and I878, which associate with NSP5, as demonstrated by binding assays, but support
366 neither VLS formation nor NSP5 hyperphosphorylation. Moreover, VP2 L124A impairs
367 VLS formation and NSP5 hyperphosphorylation in either NSP5 from RV strains OSU or
368 SA11. This outcome was not surprising since both strains have a 95% identity (Fig 3C),
369 where the NSP5 tails (region 180-198) and CKI non-canonical phosphorylation site for
370 S67D are identically conserved.

371 Interestingly, the residue L124 faces towards the VP2 inner central domains (data
372 not shown), and its modification to alanine affects VLS formation, the direct association
373 with NSP5, and the NSP5 phosphorylation state. Therefore, it suggests that the VP2-
374 NSP5 interaction interface may impede core assembly to favor viroplasm formation and
375 allow the packaging of genome segments. We show that NSP5 can associate with VP2
376 through its tail region (residues 180-198). This finding is not surprising since the role of
377 NSP5 tail has previously been described to play a role in association with other viral
378 proteins, including NSP2 (9, 35), NSP6 (12), and VP1 (23) and even as a self-
379 oligomerization domain (12, 44).

380 Collectively, our data show that NSP5-VP2 interaction and VLS formation are
381 immediate prior steps to the NSP5 hyperphosphorylation. In support of this viewpoint,
382 we provide data showing that: i) a hyperphosphorylated NSP5 (NSP5 S67D) is not
383 sufficient to form VLS with VP2 L124A, ii) NSP5 S67D does not bind VP2 L124A, iii)

384 VP2 L124A does not hyperphosphorylate wt NSP5, and iv) NSP5/S67A forms VLS with
385 wt VP2 (7). Our conclusion then provides additional insights into the molecular
386 mechanism previously proposed (44, 58) for the formation of viroplasms and subsequent
387 NSP5 hyperphosphorylation. This mechanistic interpretation is consistent with previous
388 observations that viroplasm formation requires a phosphorylation cascade triggered by
389 NSP2, which depends on CK1-alpha (43, 44, 59). Also, it is consistent with the fact that
390 NSP5 phosphorylation on S67 by CK1-alpha is a step after the interaction with VP2 ((7)
391 and this study) and NSP2 (19, 44, 58). The phosphorylation of other serines and
392 threonines of NSP5 by host cell kinases (8, 43, 60) will follow in agreement with a model
393 previously described (44, 58). Our data also suggest that the NSP5-VP2 interaction relies
394 on conserved L124 of VP2.

395 As described above, NSP2 and VP2 can both trigger NSP5 hyperphosphorylation. We
396 provide evidence also that VP2-NSP5 interaction, similar to NSP2-NSP5 interaction,
397 provides a scaffold for viroplasms formation. Impairment of the NSP5-VP2 interaction,
398 for example by VP2 L124A, abolishes the formation of VLS and viroplasms. This
399 observation is consistent with the previous model for viroplasm formation (44, 58, 59),
400 whereas NSP5 hyperphosphorylation is an initial step followed by the cytosolic inclusion
401 formation in association with both NSP2 (58) and VP2 (this study).

402 A dominant-negative refers to a mutation in a protein that adversely affects the wild-
403 type phenotype, for example, by disrupting a functional domain but retaining its
404 dimerization property. Therefore, the dominant-negative protein can dimerize with the
405 wild-type protein within the same cell, hence decreasing the activity of the wild-type

406 protein (61). We provide strong evidence that VP2 L124 works as a dominant-negative
407 protein for the formation of both VLSs and viroplasms. In this sense, we have shown that
408 i) VP2 L124 disrupts both VLS(NSP5+VP2) and VLS(NSP5+NSP2), ii) NSP5-VP2
409 interaction, in the split tripartite EGFP assay, is reduced in a dose-dependent manner with
410 VP2 L124 and iii) NSP5 and VP2 L124A neither form VLS nor bind to each other. Thus,
411 we conclude that VP2 L124A necessarily dimerizes with wt VP2 displacing NSP5 - wt
412 VP2 interaction. It is well described that NSP2 binds VP2 at several amino acid regions
413 (residues 34-86, 514-518, 664-674, and 836-845) (35). Hence, VP2 L124A also acts as
414 dominant-negative over NSP2, because VP2 L124A preserves NSP2 binding sites but did
415 not allow VLS formation. Moreover, the NSP2-VP2 interaction seems stronger than the
416 NSP5-VP2 interaction. We provide evidence for the idea that VP2 L124A can disrupt
417 viroplasms by showing that the expression of VP2 L124A interferes with RV replication
418 by damaging viroplasms. Specifically, viroplasms upon VP2 L124A expression form i)
419 aberrant inclusions, and ii) delocalize viroplasmic viral proteins in diffuse cytosolic
420 patterns or amyloid-like structures. Moreover, iii) these aberrant viroplasms are decreased
421 in viral transcription (+ssRNA synthesis) and dsRNA synthesis. Hence, VP2 L124A
422 works as a *bona fide* dominant-negative factor for the assembly and formation of
423 viroplasms. Accordingly, a point mutation on VP2 L124 to alanine on RV and possible
424 rescue by reverse genetic technique (62), would undoubtedly provide new insights into
425 the regulation of the RV life cycle. However, several attempts to rescue a recombinant
426 RV harboring VP2 L124A were performed without success, in contrast to the control
427 recombinant RV that retains wt VP2 (data not shown), reinforcing the relevance of this
428 motif in the RV replication cycle.

We consider that this study could lay the foundations for the designing of inhibitors that specifically bind at the interaction site between NSP5 and VP2.

Materials and Methods

Cells and viruses. MA104 cells (embryonic rhesus monkey kidney, ATCC®CRL-2378) and Hek293T cells (human embryonic kidney, ATCC®CRL-573) were cultured in DMEM (Dulbecco's modified Eagle's media (DMEM, Gibco®BRL) supplemented with 10% fetal calf serum (FCS) (AMIMED, BioConcept, Switzerland) and penicillin (100 U/ml)-streptomycin (100 µg/ml) (Gibco, Life Technologies). BSR-T7 cells (Baby hamster kidney, CVCL-RW96), which express T7 DNA directed RNA polymerase were cultured in DMEM supplemented with 10 % FCS, 1 mg/ml Geneticin® (G418, Thermo Fisher Scientific) and penicillin (100 U/ml) –streptomycin (100 µg/ml). The T_7 RNA polymerase recombinant vaccinia virus (strain vvT7.3) was amplified as previously described (63).

Rotavirus porcine OSU strain (G5;P[9]) was propagated in MA104 cells, as described previously (64, 65). Virus titer was determined as described previously by Eichwald et al., (10) and expressed as viroplasm-forming units (VFU) per milliliter.

Antibodies. Guinea pig anti-NSP5, guinea pig anti-NSP2, guinea pig anti-VP2, and Mouse scFV anti-NSP5 clone 1F2 were described previously (8, 19, 23, 66). Guinea pig anti-VP6 was described (10, 67). Mouse monoclonal anti-VP6 (clone 2F) was a gift from Dr. N. Mattion (CEVAN, Buenos Aires, Argentina). Rabbit anti-NSP3 was kindly provided by Dr. Susana López (UNAM, Cuernavaca, Mexico). Mouse mAb anti-VP2

(clone3E8) was kindly provided by Dr. Harry Greenberg (Stanford University, CA, USA). Mouse mAb anti-HA (clone HA-7) and mouse monoclonal anti-GAPDH (clone GAPDH-71.1) were obtained from Sigma Aldrich. Mouse mAb anti-dsRNA (clone J2) was purchased from SCICONS J2, English&Scientific consulting, Hungary. Goat anti-mouse immunoglobulin G (IgG) (H+L) conjugated to Alexa 594 and goat anti-guinea pig IgG conjugated to Alexa 488 were obtained from Molecular Probes, Invitrogen, USA. Goat polyclonal anti-mouse IgG (Fab')-peroxidase was purchased from Sigma Aldrich. Rabbit polyclonal anti-guinea pig IgG-peroxidase was purchased from Dako Cytomation, Denmark.

Plasmid constructions. The plasmids pcDNA-NSP5 porcine strain OSU (G5;P[9]), pcDNA-NSP5 simian strain SA11-4F (G3;P6[1]), pcDNA-NSP2 simian strain SA11-4F (G3;P6[1]), and pcDNA-VP2 simian strain SA11-4F (G3;P6[1]) were previously described (11, 19, 21, 23). The plasmids pCI-HA-VP2 full-length, pCI-HA-VP2ΔN81, pCI-HA-VP2ΔN103, pCI-HA-VP2ΔN135, pCI-HA-VP2ΔN159, pCI-HA-VP2ΔN181, pCI-HA-VP2ΔN203, pCI-HA-VP2ΔN316, pCI-HA-VP2ΔN588, pCI-HA-VP2ΔN720, pCI-HA-VP2ΔC81, pCI-HA-VP2ΔC203, pCI-HA-VP2ΔC316, pCI-HA-VP2ΔC588, pCI-HA-VP2ΔC721, pCI-HA-VP2ΔC755, pCI-HA-VP2ΔC840, pCI-HA-VP2(82-203), pCI-HA-VP2(204-316), pCI-HA-VP2(317-588) and pCI-HA-VP2(589-720) were obtained by PCR amplification of pcDNA-VP2 (23) using specific primers to insert flanking *Xho*I/HA-tag and *Eco*RI sites, followed by ligation into those sites in pCI-Neo (Promega). Similarly, pCI-VP2ΔN81, pCI-VP2ΔN203, pCI-VP2ΔN316, pCI-VP2ΔN588, pCI-VP2ΔN720, pCI-VP2ΔC81, pCI-VP2ΔC203, pCI-VP2ΔC316, pCI-VP2ΔC588, and pCI-

472 VP2ΔC720 were obtained by PCR amplification of pcDNA-VP2 using specific primers
473 to insert *Xho*I and *EcoR*I sites, followed by ligation into those sites in pCI-Neo.

474 The constructs pCI-H_6-NSP5, pCI-H_6-NSP5 S67D, pCI-H_6-EGFP, pCI-H_6-EGFP-T,
475 and pCI-H_6-EGFP-dom4 were obtained from PCR amplification of pcDNA-NSP5 (11),
476 pcDNA-NSP5 S67D (44), pEGFP-N1 (Clontech), p(1-EGFP-T) (9) and p(EGFP-4) (9)
477 using specific primers to insert *Xho*I/hexahistidine tag and *Not*I sites, following by
478 ligation on those sites in pCI-Neo (Promega). The construct pcDNA-H_6-Δ1Δ3 was
479 previously described (8). The constructs pCI-H_6-NSP5ΔT and pCI-H_6-Δ1Δ3ΔT were
480 obtained by PCR amplification of pcDNA-H_6-NSP5and pcDNA-H_6-Δ1Δ3 using specific
481 primers for the insertion of a *Xho*I restriction site at the 5'-end and the reverse
482 oligonucleotide primer 5'-gatcgcggccgcttagaagcacctttttcttatattt-3' for the deletion of NSP5
483 tail and insertion of Stop codon/*Not*I site at the 3'-end. The PCR fragment was ligated
484 between *Xho*I/*Not*I sites in pCI-Neo (Promega). The plasmids pCI-mCherry and
485 pcDNA3.1tn(+)-GFP1-9OPT were previously described (45, 68). The construct p10L-
486 NSP5 was obtained by PCR amplification of pcDNA-NSP5 using specific primers to
487 insert *Pac*I and *Xho*I sites, following by ligation in-frame in pcDNA3.1tn(+)GFP10+long
488 linker (45). The construct p10L-NSP5 (T) was obtained by annealing of the
489 oligonucleotides 5'-taacattgcactaagaatgaggatgaagcaagtcgcaatgcaattgatcgaagatttgtaac-3'
490 and 5'-tcgagttacaaatcttcgatcaattgcattgcgacttgcttcatcctcattcttagtgcaatgttaat-3', followed by
491 ligation into *Pac*I and *Xho*I sites of pcDNA3.1tn(+)-GFP10+long linker (45). The
492 construct p11L-VP2 was obtained by PCR amplification of pcDNA-VP2 using specific
493 primers to insert *Pac*I and *EcoR*I sites, following by ligation on those sites in
494 pcDNA3.1tn(+)-linker+GFP11(45).

pCAG-D1R (Addgene plasmid #89160) and pCAG-D12L (Addgene plasmid # 89161) were a gift from Takeshi Kobayashi (62).

Version of constructs pCDNA-VP2, pCI-HA-VP2(ΔN103) and p11L-VP2 harboring the VP2 point mutations I106A, D112A, L124A, R125A, I127A, M843A, F850A, L856A, V860A, F865A, F873A, F878A, V865A or I878A were built by insertion of point mutations using the QuickChange Site-Directed Mutagenesis kit and protocol (Agilent). All the oligonucleotides were obtained from Microsynth AG, Switzerland, and are available upon request.

Immunofluorescence. For VLS detection, 1 x 10^5 MA104 cells per well were seeded in 24 well multiwell plates over coverslip. Cells infected with vvT7.3 (3 PFU/cell) were transfected for 15 hpt in an empirically determined ratio 2:1 of NSP5 and VP2, using Lipofectamine® 2000 (Thermo Fisher Scientific) according to the manufacturer's instructions. For viroplasms detection, transfected BSR-T7 cells were infected for 5 h at an MOI of 75 VFU/cell. At the indicated time post-infection, cells were fixed in 2% paraformaldehyde in PBS for 10 min at room temperature and processed as described by Eichwald et al., 2012 (10). When indicated, images were acquired using a fluorescence microscope (Leica, DMI6000B) or a CLSM (Leica, DM550Q). Data were analyzed with Leica Application Suite (Mannheim, Germany) and Image J (version: 2.0.0-RC-69/1.52i; http://imagej.net/Contributors). Images were prepared for publication using PowerPoint (Microsoft) and Adobe Photoshop® Softwares. The intensity profile plots were obtained using Image J, ROI manager, multi-plot algorithm.

516 **Pull-down assay.** MA104 cells were infected with vvT7.3 (MOI, 3 PFU/cell), followed
517 by transfection at ratio 1:1 of two DNA plasmids using Lipofectamine® 2000 (Thermo
518 Fisher Scientific) according to manufacturer instructions. At 16 hpt, cells were processed
519 as described previously (69)

520 **Hyperphosphorylation assay.** The assay was performed as described by Eichwald *et al.*,
521 2004 (44). Briefly, $2x10^5$ cells in 12 wells multi-well plate were infected with T_7 RNA
522 polymerase recombinant vaccinia virus (vvT7.3) (63) (MOI, 3 PFU/cell) followed by
523 transfection with 2 µg of total plasmid DNA (1 µg of the substrate and 1µg activator) and
524 3 µl Lipofectamine® 2000 Transfection reagent (ThermoFisher Scientific). At 16 hpt,
525 cells were lysed in 30 µl of TNN lysis buffer (100 mM Tris-HCl pH 8.0, 250 mM NaCl,
526 0.5% Nonidet P-40 and cOmplete protease inhibitor cocktail (Roche, Switzerland)) for 10
527 min at 4˚C. Samples were harvested and centrifuged at 17'000 x *g* for 7 min at 4˚C. The
528 supernatant was analyzed by immunoblotting, as described previously (10).

529 **Lambda-phosphatase assay.** Cellular extracts were treated with lambda phosphatase, as
530 described by Eichwald *et al.*, 2004 (44). For analysis, samples were loaded in SDS-
531 polyacrylamide and analyzed by immunoblotting for the detection of NSP5 (10).

532 **Protein-protein interaction tripartite split-GFP assay.** The assay was performed as
533 previously described by Cabantous *et al.*, 2013 (45). Briefly, $5x10^4$ per well of Hek293T
534 cells are seeded in 48 multi-well plates. Cells were co-transfected by mixing 20 ng pCI-
535 mCherry, 60 ng pcDNA3.1tn(+) GFP1-9 OPT, 60 ng p10L-NSP5 and 60 ng p11L-VP2
536 using with 1µl Lipofectamine® 2000 (Thermo Fisher Scientific) in 40 µl Opti-MEM™

(Thermo Fisher Scientific) followed by 20 min incubation at room temperature. The transfection mixture was added to the cells held under 160 µl of DMEM supplemented with 10% FCS. At 24 hpt, cells were released with trypsin-EDTA, harvested in cDMEM, and centrifuged at low speed for 2 min. Cellular pellets were resuspended in FC buffer (5 mM EDTA pH 8.0, 2% FCS in PBS), filtered in cell strained snap-cap tube (BD Falcon™) and immediately acquired in a Gallios™ Flow Cytometer (Beckman Coulter, Inc). In total, 10,000 events were acquired exciting with 488 nm and 561 nm lasers followed by recording with default filters of 525/50 nm (GFP, green) and 620/30 nm (mCherry, red), respectively. Data were analyzed normalizing the number of green cells to 10'000 events on the positive red population using a Kaluza® Flow Analysis Software. The statistical analysis and plot were performed using Microsoft® Excel® for MAC 2011 Version 14.7.3. and also, Prism 8 (GraphPad Software, Inc.).

Dominant-negative assay for viroplasm formation. BSR-T7 cells ($2x10^5$) seeded in 24-well plates over coverslip were transfected with 1µg pcDNA-VP2 or pcDNA-VP2 L124A, 0.1µg pCAG-D1R and 0.1µg pCAG-D12L using Lipofectamine® 2000 according to manufacturer's instructions. At 24 hpt, cells were infected with porcine rotavirus strain OSU at indicated MOI. The virus was adsorbed for 1 h at 4˚C, followed by incubation at 37˚C. At 5 hpi, cells were fixed 2% paraformaldehyde in PBS for 10 min at room temperature and processed for immunofluorescence as described by Eichwald et al., 2012 (10). The number of cells containing viroplasms and the total number of cells per field was counted for at least 40 fields using a fluorescence microscope. The percentage of viroplasms, plot, and statistical analysis were performed with Microsoft® Excel® 2011 for MAC, version 14.7.3, and Prism 8 (GraphPad Software, Inc.).

560 **Detection of RNA synthesis in viroplasm.** BSR-T7 cells ($2x10^5$), seeded over coverslip
561 in 24-well plate, were transfected for expression of wt VP2 and VP2 L124A, as described
562 above. At 24 hpt, cells were infected with porcine RV strain OSU at MOI of 75 VFU/cell.
563 The virus was adsorbed for 1 h at 4˚C, followed by incubation at 37˚C. BrUTP (5-
564 Bromouridine 5'-triphosphate sodium salt, Sigma-Aldrich) incorporation was performed
565 as described previously by Silvestri et al., 2004 (46) with some modifications. Briefly,
566 cells were pretreated for 30 min with 10 µM actinomycin D (GeneTex) in 500 µl serum-
567 free medium starting at 4 hpi. At 4.5 hpi, cells were transfected with a mixture containing
568 1 mM BrUTP, 10 µM actinomycin D and 20 µl of Lipofectamine® 2000 transfection
569 reagent (ThermoFisher Scientific) in 500 µl Opti-MEM reduced serum medium
570 (ThermoFisher Scientific) and incubated for 1 h at 37˚C and 5% CO_2. The cells were
571 immediately fixed in 2% paraformaldehyde in PBS for 10 min at room temperature and
572 processed for immunofluorescence by staining with Alexa Fluor® 488 anti-BrdU clone
573 3D4 (diluted 1:50, BioLegend®) and guinea pig anti-NSP5 (1:200) followed by a
574 secondary antibody conjugated to rhodamine isothiocyanate (RITC). Images were
575 subsequently acquired at CLSM (Leica, DM550Q) and images analyzed using Imaris File
576 Converter 9.0.0 and Image J (version: 2.0.0-RC-69/1.52P; http://imagej.net/Contributors).
577 Images were prepared for publication using PowerPoint (Microsoft) and Adobe
578 Photoshop® Softwares.

579 **Sequence Alignments**. To identify highly conserved amino acids among cogent proteins
580 of all RV species, an alignment for two VP2 (simian strain SA11) regions (aa 103-135
581 and aa 840-880) of all VP2 available in the protein depository of the NCBI was
582 performed using multiple sequences alignment Clustal W (70) combined with MAFFT

583 software (71). The obtained alignments were further processed using Jalview software
584 (72). The following selected sequences from rotavirus species (A-H) are represented in
585 the alignments (species, strain, host and GenBank version accession number listed for
586 each): RVA_K9 (ca)(EU7089240); RVA_SA11_lab (si)(MK184911); RVA_SA11-H96
587 (si) (NC_011506); RVA_Vanderbilt_VU08-09-24 (hu) (JF491072);
588 RVA_Vanderbilt_VU08-09-25 (hu)(JF491082); RVA_Vanderbilt_VU05-06-15
589 (hu)(JF490598); RVA_Vanderbilt_VU06-07-29 (hu)(JF490852); RVA_Wa
590 (hu)(X14942); RVA_PO-13(av)(AB009630); RVA_EB(mu)(HQ540508);
591 RVA_02V0002G3 (av)(FJ169854); RVA_Cowden (po)(M74217); RVA_OSU
592 (po)(ADE44253); RVB_WH-1 (hu)(AY539859); RVB_ADRV (hu)(M91433);
593 RVB_Bang373(hu)(NC_021545); RVB_IDIRg2 (ra)(U00673); RVB_RUBV226
594 (bo)(GQ358717); RVC_Bristol (hu)(NC_007546); RVD_05V0049/DEU/2003 (av)
595 (YP_003896047); RVF_03V0568/DEU/2003 (av)(NC_021626); RVG_HK18
596 (av)(KC876011); RVG_03V0567/DEU/2003 (av)(NC_021580);
597 RVH_MRC_DPRU1575 (po) (KT962028); and RVH_J19 (hu) (DQ113898). The
598 indicated hosts are: ca, canine; si, simian; hu, human; av, avian; mu, murine; po, porcine;
599 ra, rabbit; bo, bovine.

600 **Acknowledgments**

601 We are grateful to Luca Murer and Prof. Jovan Pavlovic for providing the
602 tripartite split GFP plasmids. We want to thank Prof. Ohad Medalia for his support in the
603 calculated models of VP2. Also, we want to thank Guido Papa and Oscar Burrone for
604 their help with RV reverse genetics. We thank Claudio Aguilar and Jakub Kubacki for
605 their valuable comments and criticism of the manuscript.

This work was supported by a private donation of the late Prof. Dr. Robert Wyler to M.A. (F-52601-10-01) and the University of Zurich. The funders had no role in study design, data collection, and interpretation, or the decision to submit the work for publication.

Conflict of interest

The authors declare that they have no conflict of interest

References

1. Troeger C, Khalil IA, Rao PC, Cao S, Blacker BF, Ahmed T, Armah G, Bines JE, Brewer TG, Colombara DV, Kang G, Kirkpatrick BD, Kirkwood CD, Mwenda JM, Parashar UD, Petri WA, Riddle MS, Steele AD, Thompson RL, Walson JL, Sanders JW, Mokdad AH, Murray CJL, Hay SI, Reiner RC. 2018. Rotavirus vaccination and the global burden of rotavirus diarrhea among children younger than 5 years. JAMA Pediatr 172:958-965.
2. McClain B, Settembre E, Temple BR, Bellamy AR, Harrison SC. 2010. X-ray crystal structure of the rotavirus inner capsid particle at 3.8 A resolution. J Mol Biol 397:587-99.
3. Periz J, Celma C, Jing B, Pinkney JN, Roy P, Kapanidis AN. 2013. Rotavirus mRNAS are released by transcript-specific channels in the double-layered viral capsid. Proc Natl Acad Sci U S A 110:12042-7.
4. Trask SD, McDonald SM, Patton JT. 2012. Structural insights into the coupling of virion assembly and rotavirus replication. Nat Rev Microbiol 10:165-77.
5. Berkova Z, Crawford SE, Trugnan G, Yoshimori T, Morris AP, Estes MK. 2006. Rotavirus NSP4 induces a novel vesicular compartment regulated by calcium and associated with viroplasms. J Virol 80:6061-71.
6. Patton JT, Silvestri LS, Tortorici MA, Vasquez-Del Carpio R, Taraporewala ZF. 2006. Rotavirus genome replication and morphogenesis: role of the viroplasm. Curr Top Microbiol Immunol 309:169-87.
7. Contin R, Arnoldi F, Campagna M, Burrone OR. 2010. Rotavirus NSP5 orchestrates recruitment of viroplasmic proteins. J Gen Virol 91:1782-93.
8. Eichwald C, Vascotto F, Fabbretti E, Burrone OR. 2002. Rotavirus NSP5: mapping phosphorylation sites and kinase activation and viroplasm localization domains. J Virol 76:3461-70.

9. Eichwald C, Rodriguez JF, Burrone OR. 2004. Characterization of rotavirus NSP2/NSP5 interactions and the dynamics of viroplasm formation. J Gen Virol 85:625-34.
10. Eichwald C, Arnoldi F, Laimbacher AS, Schraner EM, Fraefel C, Wild P, Burrone OR, Ackermann M. 2012. Rotavirus viroplasm fusion and perinuclear localization are dynamic processes requiring stabilized microtubules. PLoS One 7:e47947.
11. Fabbretti E, Afrikanova I, Vascotto F, Burrone OR. 1999. Two non-structural rotavirus proteins, NSP2 and NSP5, form viroplasm-like structures *in vivo*. J Gen Virol 80 (Pt 2):333-9.
12. Torres-Vega MA, González RA, Duarte M, Poncet D, López S, Arias CF. 2000. The C-terminal domain of rotavirus NSP5 is essential for its multimerization, hyperphosphorylation and interaction with NSP6. J Gen Virol 81:821-30.
13. Cabral-Romero C, Padilla-Noriega L. 2006. Association of rotavirus viroplasms with microtubules through NSP2 and NSP5. Mem Inst Oswaldo Cruz 101:603-11.
14. Criglar JM, Hu L, Crawford SE, Hyser JM, Broughman JR, Prasad BV, Estes MK. 2014. A novel form of rotavirus NSP2 and phosphorylation-dependent NSP2-NSP5 interactions are associated with viroplasm assembly. J Virol 88:786-98.
15. Martin D, Duarte M, Lepault J, Poncet D. 2010. Sequestration of free tubulin molecules by the viral protein NSP2 induces microtubule depolymerization during rotavirus infection. J Virol 84:2522-32.
16. Afrikanova I, Miozzo MC, Giambiagi S, Burrone O. 1996. Phosphorylation generates different forms of rotavirus NSP5. J Gen Virol 77 (Pt 9):2059-65.
17. Poncet D, Lindenbaum P, L'Haridon R, Cohen J. 1997. *In vivo* and *in vitro* phosphorylation of rotavirus NSP5 correlates with its localization in viroplasms. J Virol 71:34-41.
18. González SA, Burrone OR. 1991. Rotavirus NS26 is modified by addition of single O-linked residues of N-acetylglucosamine. Virology 182:8-16.
19. Afrikanova I, Fabbretti E, Miozzo MC, Burrone OR. 1998. Rotavirus NSP5 phosphorylation is up-regulated by interaction with NSP2. J Gen Virol 79 (Pt 11):2679-86.
20. Contin R, Arnoldi F, Mano M, Burrone OR. 2011. Rotavirus replication requires a functional proteasome for effective assembly of viroplasms. J Virol 85:2781-92.
21. Campagna M, Eichwald C, Vascotto F, Burrone OR. 2005. RNA interference of rotavirus segment 11 mRNA reveals the essential role of NSP5 in the virus replicative cycle. J Gen Virol 86:1481-7.
22. López T, Rojas M, Ayala-Bretón C, López S, Arias CF. 2005. Reduced expression of the rotavirus NSP5 gene has a pleiotropic effect on virus replication. J Gen Virol 86:1609-17.
23. Arnoldi F, Campagna M, Eichwald C, Desselberger U, Burrone OR. 2007. Interaction of rotavirus polymerase VP1 with nonstructural protein NSP5 is stronger than that with NSP2. J Virol 81:2128-37.
24. Berois M, Sapin C, Erk I, Poncet D, Cohen J. 2003. Rotavirus nonstructural protein NSP5 interacts with major core protein VP2. J Virol 77:1757-63.

682 25. Vende P, Taraporewala ZF, Patton JT. 2002. RNA-binding activity of the
683 rotavirus phosphoprotein NSP5 includes affinity for double-stranded RNA. J
684 Virol 76:5291-9.
685 26. Jiang X, Jayaram H, Kumar M, Ludtke SJ, Estes MK, Prasad BV. 2006.
686 Cryoelectron microscopy structures of rotavirus NSP2-NSP5 and NSP2-RNA
687 complexes: implications for genome replication. J Virol 80:10829-35.
688 27. Martin D, Charpilienne A, Parent A, Boussac A, D'Autreaux B, Poupon J, Poncet
689 D. 2013. The rotavirus nonstructural protein NSP5 coordinates a [2Fe-2S] iron-
690 sulfur cluster that modulates interaction to RNA. FASEB J 27:1074-83.
691 28. McDonald SM, Patton JT. 2011. Rotavirus VP2 core shell regions critical for viral
692 polymerase activation. J Virol 85:3095-105.
693 29. Campagna M, Marcos-Villar L, Arnoldi F, de la Cruz-Herrera CF, Gallego P,
694 González-Santamaría J, González D, Lopitz-Otsoa F, Rodriguez MS, Burrone
695 OR, Rivas C. 2013. Rotavirus viroplasm proteins interact with the cellular
696 SUMOylation system: implications for viroplasm-like structure formation. J Virol
697 87:807-17.
698 30. Patton JT, Jones MT, Kalbach AN, He YW, Xiaobo J. 1997. Rotavirus RNA
699 polymerase requires the core shell protein to synthesize the double-stranded RNA
700 genome. J Virol 71:9618-26.
701 31. Lawton JA, Zeng CQ, Mukherjee SK, Cohen J, Estes MK, Prasad BV. 1997.
702 Three-dimensional structural analysis of recombinant rotavirus-like particles with
703 intact and amino-terminal-deleted VP2: implications for the architecture of the
704 VP2 capsid layer. J Virol 71:7353-60.
705 32. Li Z, Baker ML, Jiang W, Estes MK, Prasad BV. 2009. Rotavirus architecture at
706 subnanometer resolution. J Virol 83:1754-66.
707 33. Zhang X, Settembre E, Xu C, Dormitzer PR, Bellamy R, Harrison SC, Grigorieff
708 N. 2008. Near-atomic resolution using electron cryomicroscopy and single-
709 particle reconstruction. Proc Natl Acad Sci U S A 105:1867-72.
710 34. Charpilienne A, Lepault J, Rey F, Cohen J. 2002. Identification of rotavirus VP6
711 residues located at the interface with VP2 that are essential for capsid assembly
712 and transcriptase activity. J Virol 76:7822-31.
713 35. Viskovska M, Anish R, Hu L, Chow DC, Hurwitz AM, Brown NG, Palzkill T,
714 Estes MK, Prasad BV. 2014. Probing the sites of interactions of rotaviral proteins
715 involved in replication. J Virol 88:12866-81.
716 36. Zeng CQ, Estes MK, Charpilienne A, Cohen J. 1998. The N terminus of rotavirus
717 VP2 is necessary for encapsidation of VP1 and VP3. J Virol 72:201-8.
718 37. Labbé M, Baudoux P, Charpilienne A, Poncet D, Cohen J. 1994. Identification of
719 the nucleic acid binding domain of the rotavirus VP2 protein. J Gen Virol 75 (Pt
720 12):3423-30.
721 38. Ding K, Celma CC, Zhang X, Chang T, Shen W, Atanasov I, Roy P, Zhou ZH.
722 2019. *In situ* structures of rotavirus polymerase in action and mechanism of
723 mRNA transcription and release. Nat Commun 10:2216.
724 39. Estrozi LF, Settembre EC, Goret G, McClain B, Zhang X, Chen JZ, Grigorieff N,
725 Harrison SC. 2013. Location of the dsRNA-dependent polymerase, VP1, in
726 rotavirus particles. J Mol Biol 425:124-32.

40. Jenni S, Salgado EN, Herrmann T, Li Z, Grant T, Grigorieff N, Trapani S, Estrozi LF, Harrison SC. 2019. In situ Structure of Rotavirus VP1 RNA-Dependent RNA Polymerase. J Mol Biol 431:3124-3138.
41. Laimbacher AS, Esteban LE, Castello AA, Abdusetir Cerfoglio JC, Argüelles MH, Glikmann G, D'Antuono A, Mattion N, Berois M, Arbiza J, Hilbe M, Schraner EM, Seyffert M, Dresch C, Epstein AL, Ackermann M, Fraefel C. 2012. HSV-1 amplicon vectors launch the production of heterologous rotavirus-like particles and induce rotavirus-specific immune responses in mice. Mol Ther 20:1810-20.
42. Boudreaux CE, Vile DC, Gilmore BL, Tanner JR, Kelly DF, McDonald SM. 2013. Rotavirus core shell subdomains involved in polymerase encapsidation into virus-like particles. J Gen Virol 94:1818-26.
43. Campagna M, Budini M, Arnoldi F, Desselberger U, Allende JE, Burrone OR. 2007. Impaired hyperphosphorylation of rotavirus NSP5 in cells depleted of casein kinase 1alpha is associated with the formation of viroplasms with altered morphology and a moderate decrease in virus replication. J Gen Virol 88:2800-10.
44. Eichwald C, Jacob G, Muszynski B, Allende JE, Burrone OR. 2004. Uncoupling substrate and activation functions of rotavirus NSP5: phosphorylation of Ser-67 by casein kinase 1 is essential for hyperphosphorylation. Proc Natl Acad Sci U S A 101:16304-9.
45. Cabantous S, Nguyen HB, Pedelacq JD, Koraïchi F, Chaudhary A, Ganguly K, Lockard MA, Favre G, Terwilliger TC, Waldo GS. 2013. A new protein-protein interaction sensor based on tripartite split-GFP association. Sci Rep 3:2854.
46. Silvestri LS, Taraporewala ZF, Patton JT. 2004. Rotavirus replication: plus-sense templates for double-stranded RNA synthesis are made in viroplasms. J Virol 78:7763-74.
47. Spencer E, Arias ML. 1981. *In vitro* transcription catalyzed by heat-treated human rotavirus. J Virol 40:1-10.
48. Schönborn J, Oberstrass J, Breyel E, Tittgen J, Schumacher J, Lukacs N. 1991. Monoclonal antibodies to double-stranded RNA as probes of RNA structure in crude nucleic acid extracts. Nucleic Acids Res 19:2993-3000.
49. McDonald SM, Patton JT. 2011. Assortment and packaging of the segmented rotavirus genome. Trends Microbiol 19:136-44.
50. Ahmed K, Nakagomi T, Nakagomi O. 2005. Isolation and molecular characterization of a naturally occurring non-structural protein 5 (NSP5) gene reassortant of group A rotavirus of serotype G2P[4] with a long RNA pattern. J Med Virol 77:323-30.
51. Kojima K, Taniguchi K, Urasawa T, Urasawa S. 1996. Sequence analysis of normal and rearranged NSP5 genes from human rotavirus strains isolated in nature: implications for the occurrence of the rearrangement at the step of plus strand synthesis. Virology 224:446-52.
52. Komoto S, Kanai Y, Fukuda S, Kugita M, Kawagishi T, Ito N, Sugiyama M, Matsuura Y, Kobayashi T, Taniguchi K. 2017. Reverse genetics system demonstrates that rotavirus nonstructural protein NSP6 is not essential for viral replication in cell culture. J Virol 91.

53. Wu H, Taniguchi K, Urasawa T, Urasawa S. 1998. Serological and genomic characterization of human rotaviruses detected in China. J Med Virol 55:168-76.
54. Prasad BV, Wang GJ, Clerx JP, Chiu W. 1988. Three-dimensional structure of rotavirus. J Mol Biol 199:269-75.
55. Yeager M, Dryden KA, Olson NH, Greenberg HB, Baker TS. 1990. Three-dimensional structure of rhesus rotavirus by cryoelectron microscopy and image reconstruction. J Cell Biol 110:2133-44.
56. Glück S, Buttafuoco A, Meier AF, Arnoldi F, Vogt B, Schraner EM, Ackermann M, Eichwald C. 2017. Rotavirus replication is correlated with S/G2 interphase arrest of the host cell cycle. PLoS One 12:e0179607.
57. Settembre EC, Chen JZ, Dormitzer PR, Grigorieff N, Harrison SC. 2011. Atomic model of an infectious rotavirus particle. EMBO J 30:408-16.
58. Papa G, Venditti L, Arnoldi F, Schraner EM, Potgieter C, Borodavka A, Eichwald C, Burrone OR. 2019. Recombinant rotaviruses rescued by reverse genetics reveal the role of NSP5 hyperphosphorylation in the assembly of viral factories. J Virol. DOI: 10.1128/JVI.01110-19
59. Criglar JM, Anish R, Hu L, Crawford SE, Sankaran B, Prasad BVV, Estes MK. 2018. Phosphorylation cascade regulates the formation and maturation of rotaviral replication factories. Proc Natl Acad Sci U S A 115:E12015-E12023.
60. Sotelo PH, Schümann M, Krause E, Chnaiderman J. 2010. Analysis of rotavirus non-structural protein NSP5 by mass spectrometry reveals a complex phosphorylation pattern. Virus Res 149:104-8.
61. Sheppard D. 1994. Dominant negative mutants: tools for the study of protein function in vitro and in vivo. Am J Respir Cell Mol Biol 11:1-6.
62. Kanai Y, Komoto S, Kawagishi T, Nouda R, Nagasawa N, Onishi M, Matsuura Y, Taniguchi K, Kobayashi T. 2017. Entirely plasmid-based reverse genetics system for rotaviruses. Proc Natl Acad Sci U S A 114:2349-2354.
63. Fuerst TR, Niles EG, Studier FW, Moss B. 1986. Eukaryotic transient-expression system based on recombinant vaccinia virus that synthesizes bacteriophage T7 RNA polymerase. Proc Natl Acad Sci U S A 83:8122-6.
64. Arnold M, Patton JT, McDonald SM. 2009. Culturing, storage, and quantification of rotaviruses. Curr Protoc Microbiol Chapter 15:Unit 15C.3.
65. Estes MK, Graham DY, Gerba CP, Smith EM. 1979. Simian rotavirus SA11 replication in cell cultures. J Virol 31:810-5.
66. Petris G, Bestagno M, Arnoldi F, Burrone OR. 2014. New tags for recombinant protein detection and O-glycosylation reporters. PLoS One 9:e96700.
67. Eichwald C, De Lorenzo G, Schraner EM, Papa G, Bollati M, Swuec P, de Rosa M, Milani M, Mastrangelo E, Ackermann M, Burrone OR, Arnoldi F. 2018. Identification of a small molecule that compromises the structural integrity of viroplasms and rotavirus double-layered particles. J Virol 92.
68. Eichwald C, Ackermann M, Nibert ML. 2018. The dynamics of both filamentous and globular mammalian reovirus viral factories rely on the microtubule network. Virology 518:77-86.
69. Eichwald C, Kim J, Nibert ML. 2017. Dissection of mammalian orthoreovirus µ2 reveals a self-associative domain required for binding to microtubules but not to factory matrix protein µNS. PLoS One 12:e0184356.

70. Larkin MA, Blackshields G, Brown NP, Chenna R, McGettigan PA, McWilliam H, Valentin F, Wallace IM, Wilm A, Lopez R, Thompson JD, Gibson TJ, Higgins DG. 2007. Clustal W and Clustal X version 2.0. Bioinformatics 23:2947-8.
71. Katoh K, Rozewicki J, Yamada KD. 2019. MAFFT online service: multiple sequence alignment, interactive sequence choice and visualization. Brief Bioinform 20:1160-1166.
72. Waterhouse AM, Procter JB, Martin DM, Clamp M, Barton GJ. 2009. Jalview Version 2--a multiple sequence alignment editor and analysis workbench. Bioinformatics 25:1189-91.

Figure Legends

Figure 1. VP2 amino acid regions 103-134 and 840-880 are necessary for VLS formation. (A) Schematic representation of VP2 deletion mutants fused to an HA-tag at the N-terminus (not to scale). The dashed lines correspond to deleted regions. Positive (+) or negative (-) VLS phenotype is indicated at the right. N-terminal (NTD), central, apical, and dimerization (dim) VP2 tertiary domains are indicated. (B) Representative photomicrographs of MA104 cells expressing the indicated N- and C-terminal of HA-VP2 deletion mutants alone (-NSP5 panel) or together with NSP5 (+ NSP5 panel). At 16 hpt, cells were fixed and immunostained for detection of HA-VP2 deletion mutant (anti-HA, red) and NSP5 (anti-NSP5, green). A merged image is shown in the right column. Nuclei were stained with DAPI (blue). White arrows point to VLSs. Scale bar is 10 µm.

Figure 2. VP2 residues L124, V865, and I878 are required for VLS formation. Alignment of rotavirus VP2 (strain SA11) amino acid region 103-135 (A) and region 840-880 (B). The VP2 amino acid sequences of several representative virus strains are shown. GenBank accession numbers are listed in Materials and Methods. Members of rotavirus families A to H are indicated. Highly conserved amino acids are shown in dark

blue. Amino acid residues mutated to alanine are indicated on the top. (-) indicates deletion. (B) Immunofluorescence of MA104 cells expressing wt VP2 or point mutations alone (-NSP5 column) or together with NSP5 (+ NSP5 panel). At 16 hpt, cells were fixed, and VLSs were detected by immunostaining of HA-VP2 (anti-HA, red) or VP2 (anti-VP2, green) with NSP5 (anti-NSP5, green or red). A merged image is shown in the right column. Nuclei were stained with DAPI (blue). Scale bar is 10 µm.

Figure 3. VLS formation and triggering of NSP5 hyperphosphorylation from cognate and non-cognate strains are sensitive to VP2 L124A. (A) Immunofluorescence of MA104 cells for detection of VLS composed of NSP5 from simian strain SA11 (top panel) or NSP5 from porcine strain OSU (bottom panel) in co-expression with VP2 from simian strain SA11 wt or L124A. At 16 hpt, cells were fixed and immunostained for detection of NSP5 (anti-NSP5, green) and VP2 (anti-VP2, red). A merged image is at the right column of each panel. Nuclei were stained with DAPI (blue). Scale bar is 10 µm. (B) Immunoblotting of lysates from MA104 cells co-expressing NSP5 OSU (lanes 1-3) or NSP5-SA11 (lanes 4-6) with VP2-SA11 wt (lanes 2 and 5) or L124A (lanes 4 and 6). The membranes were incubated with specific antibodies for the detection of NSP5. Alpha-tubulin was used as a loading control. The red brackets indicate NSP5 hyperphosphorylation. (C) Sequence alignment of NSP5 from simian strain SA11 and porcine strain OSU. The identity between the two proteins corresponds to 94.95%. Non-canonical casein kinase I alpha region and oligomerization tail are labeled in blue and red, respectively.

Figure 4. VP2 residues L124, V865, and I878 are necessary to trigger NSP5 hyperphosphorylation. Co-expression of VP2 N-terminus (lanes 3-7) (A) or C-terminus

(lanes 3-7) (B) deletion mutants with NSP5. NSP5 alone (lane 1) or in co-expression with wt VP2 (fl; lane 2) is shown. NSP5 in cellular extracts was detected by immunoblot. Alpha-tubulin was used as a loading control. (C) Immunoblotting of total cellular lysates expressing NSP5 alone (lane 1) or in co-expression with VP2 wt (lane 2) or point mutations (lanes 3 to 5). NSP5 hyperphosphorylation was detected with anti-NSP5, and VP2 was detected with anti-VP2. Alpha-tubulin was used as a loading control. (D) λ-Phosphatase treatment of NSP5 co-expressed with empty vector (-), wt VP2, or VP2 L124A. NSP5 is visualized by immunoblotting. Untreated (-) and treated (+) samples are indicated. Red brackets indicate the NSP5 mobility shift. The red dots show the NSP5 unphosphorylated isoform. (E) Schematic representation of point mutations in wt NSP5 and NSP5 S67D. S to D modification is indicated in red (44). (F) Immunofluorescence of MA104 cells for detection of VLSs formed with wt or mutant NSP5 with wt VP2 (upper panel) or VP2 L124A (lower panel). At 16 hpt, cells were fixed and immunostained for detection of VLS with anti-NSP5 (green) and anti-VP2 (red). Nuclei were stained with DAPI (blue). Scale bar is 10 µm. (G) Immunoblotting of total cellular lysates expressing wt NSP5 (lanes 1-3) or NSP5 S67D (lanes 4-6) with wt VP2 or VP2 L124A. When indicated, the membranes were incubated with anti-VP2 or anti-NSP5. The brackets indicate NSP5 hyperphosphorylation smear. (H) Pull-down assay of cell extracts co-expressing H_6-NSP5 (lanes 1-2 and 5-6) or H_6-NSP5 S67D (lanes 3-4 and 7-8) with wt VP2 (lanes 1, 3, 5 and 7) or VP2 L124A (lanes 2, 4, 6 and 8). Samples were detected by immunoblot using anti-NSP5 and anti-VP2 antibodies. Input (lanes 1-4) and elution fractions are indicated (lanes 5-8).

888 **Figure 5. NSP5 tail and VP2 residues L124 and I878 are required for their**
889 **association.** (A) Immunoblotting of nickel resin pulled down cellular extracts co-
890 expressing histidine-tagged NSP5 (H_6-NSP5) with wt VP2 or harboring the indicated
891 point mutation (ce, cellular extract input; ft, flow-through and el, column eluate). (B)
892 Schematic representation of Histidine tagged (H6)-NSP5 deletion mutants used in (C, D,
893 and E). Amino acid residues delimiting the NSP5 regions are labeled at the top. Not to
894 scale. (C) Immunoblotting of pulled-down lysates from cells co-expressing H_6-NSP5
895 (lanes 1-3) or H_6-NSP5ΔT (lanes 4-6) with wt VP2. (D) Immunoblotting of pulled-down
896 lysates from cells co-expressing wt VP2 with H_6-Δ1Δ3 (lanes 1-3) or H_6-Δ1Δ3ΔT (lanes
897 4-6). (E) Immunoblotting of pulled-down lysates from cells co-expressing VP2 L124A
898 (lanes 1-3) or wt VP2 (lanes 4-6) with H_6-Δ1Δ3. When indicated the membranes were
899 incubated with anti-VP2 or anti-NSP5 antibodies. (F) Schematic representation of H_6-
900 EGFP fused to NSP5 regions used in assay from E. Not to scale. (E) Plot showing the wt
901 VP2 binding to H_6-EGFP fused to NSP5 C-terminus regions. Data are represented as
902 mean ± SD of four independent experiments. Student's t-test (*), $p<0.05$.

903 **Figure 6. NSP5 and VP2 interact directly.** (A) Schematic representation of NSP5-VP2
904 interaction sensor base in the tripartite split-GFP association. GFP beta strands 10 and 11
905 are fused to bait, NSP5 or T-NSP5, and prey, wt VP2 or point mutations. The detector
906 fragment, GFP 1-9, is added separately. When protein interaction occurs (*i*) GFP10 and
907 GFP11 are tethered and spontaneously associate with the GFP 1-9 fragment to form a
908 full-length GFP, which fluoresces in green. If the bait and prey do not interact (*ii*), GFP10
909 and GFP11 are not tethered, and entropy is too high to allow complementation with GFP
910 1-9, and therefore, no green fluorescence is detected. (B) The NSP5-VP2 direct binding

plot is showing the normalized number of green fluorescent cells for the indicated bait-prey pairs. The samples showing a single partner were expressed together with GFP10 or GFP11. (C) Competition assay plot for NSP5 binding between wt VP2 and VP2 L124A. In (B-C), data shows the mean ± SEM of six independent experiments. Two-tailed, non-parametric Mann-Whitney test; (***) $p<0.001$ and (*) $p<0.05$ compared to NSP5-VP2 green fluorescence.

Figure 7. VP2 L124A disrupts VLS formation. Immunofluorescence of VLS formation, MA104 cells were expressing NSP5 with HA-VP2 plus increasing amounts (0.25, 0.5 and 1 µg) of either wt VP2 (A) or VP2 L124A (B). At 16 hpt, cells were fixed and immunostained for VLS by detecting NSP5 (anti-NSP5, red) and HA-VP2 (anti-HA, green). Nuclei were stained with DAPI (blue). White arrowheads denote impaired VLS. Scale bar is 10 µm. (C) Immunofluorescence of VLS(NSP5+NSP2) alone (upper panel), with wt VP2 (middle panel) or with VP2 L124A (lower panel). At 16 hpt, MA104 cells were fixed and immunostained for the VLS with anti-NSP5 (red) and anti-NSP2 or anti-VP2 (green). Nuclei were stained with DAPI (blue). A merged image is shown at the right of each panel. The white arrowheads point to misshaped VLS. Scale bar is 10 µm.

Figure 8. Viroplasms are damaged by VP2 L124A expression. (A) Immunoblotting of lysates from BSR-T7 cells expressing wt VP2 (lane 2) and VP2 L124A (lane 3) at 48 hpt. OSU virus particles were used as a positive control (lane 1). (B) Plot of the percentage of cells showing viroplasms when expressing either wt VP2 or VP2 L124A. A cell was considered as viroplasm positive when detecting anti-NSP5 cytosolic inclusions. Data are represented as mean ± SD of three independent experiments; two-tailed unpaired

933 Student's t-test, (***) p<0.001, n>1500 cells per experimental point. (C) Representative
934 immunofluorescence images comparing viroplasm morphologies (5 hpi) (anti-NSP5,
935 green) of cells expressing VP2 L124A (upper panel, frames *i, ii, iii* and *iv*) or wt VP2
936 (lower panel, frames *v* and *vi*). Nuclei were stained with DAPI (blue). Scale bar is 10 µm.
937 (D) Confocal immunofluorescence of RV proteins of cells expressing wt VP2 (left panel)
938 or VP2 L124A (right panel). At 24 hpt, BSR-T7 cells were RV-infected (MOI, 75
939 VFU/cell). At 5 hpi, cells were fixed and immunostained for the detection of NSP5 (anti-
940 NSP5, green or red), VP2 (anti-VP2, green), NSP2 (anti-NSP2, green), VP6 (anti-VP6,
941 red) and NSP3 (anti-NSP3, red) and VP6, VP7 and VP4 (anti-RV, green). Nuclei were
942 stained with DAPI (blue). Scale bar is 5 µm.

943 **Figure 9. VP2 L124A expression decreases viral transcription and replication of**
944 **viroplasms.** (A) At 24 hpt for expression of wt VP2 (upper row) and VP2 L124A (lower
945 row), BSR-T7 cells were RV-infected (MOI, 75 VFU/cell). At 4 hpi, cells were treated
946 with 10 µM actinomycin D for 30 min and then transfected for 1h with 1mM BrUTP
947 (+BrUTP) or not (-BrUTP) before fixation. Cells were immunostained for BrUTP
948 incorporation (anti-BrdU, green) and viroplasms detection (anti-NSP5, red). Nuclei were
949 stained with DAPI (blue). Scale bar is 5 µm. (B) Confocal immunofluorescence of BSR-
950 T7 cells alone, expressing wt VP2 or VP2 L124A followed at 24 hpt by RV-infection
951 (MOI, 150 VFU/cell). At 5 hpi, cells were fixed and immunostained for detection of
952 dsRNA (anti-dsRNA, red) and viroplasms (anti-NSP5, green). Nuclei were stained with
953 DAPI (blue). N.T., non-transfected cells. Scale bar is 5 µm. (C) Intensity profile plot of
954 dsRNA (red line) and viroplasms (green line) of the indicated linear region of interest of
955 cells from B.

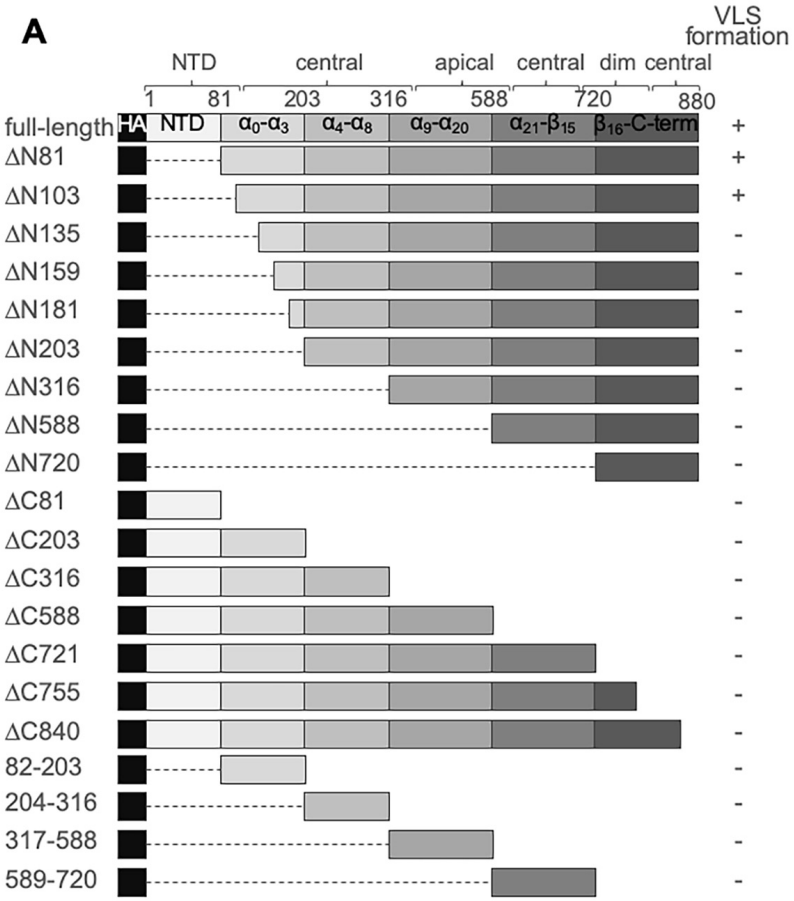

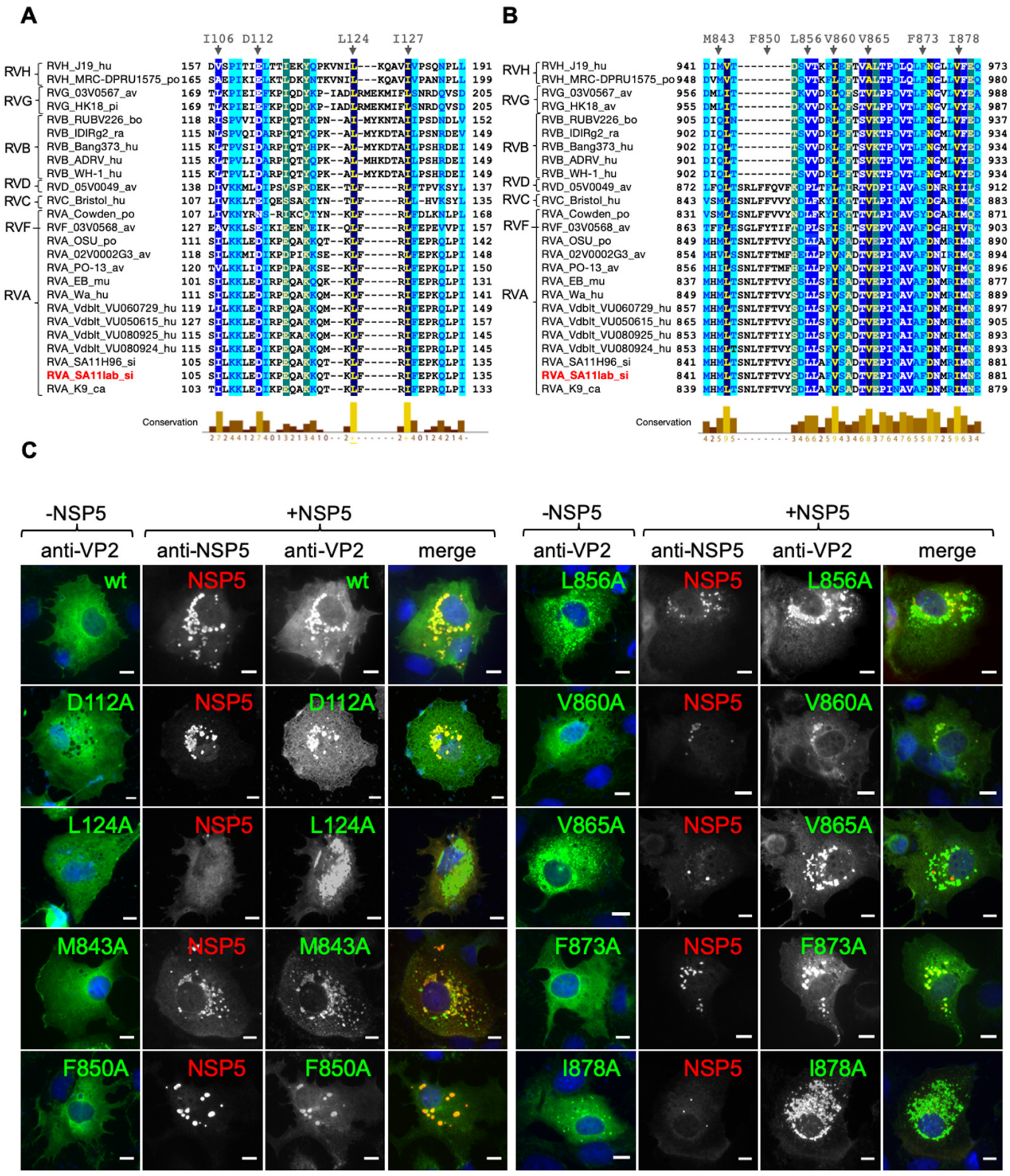

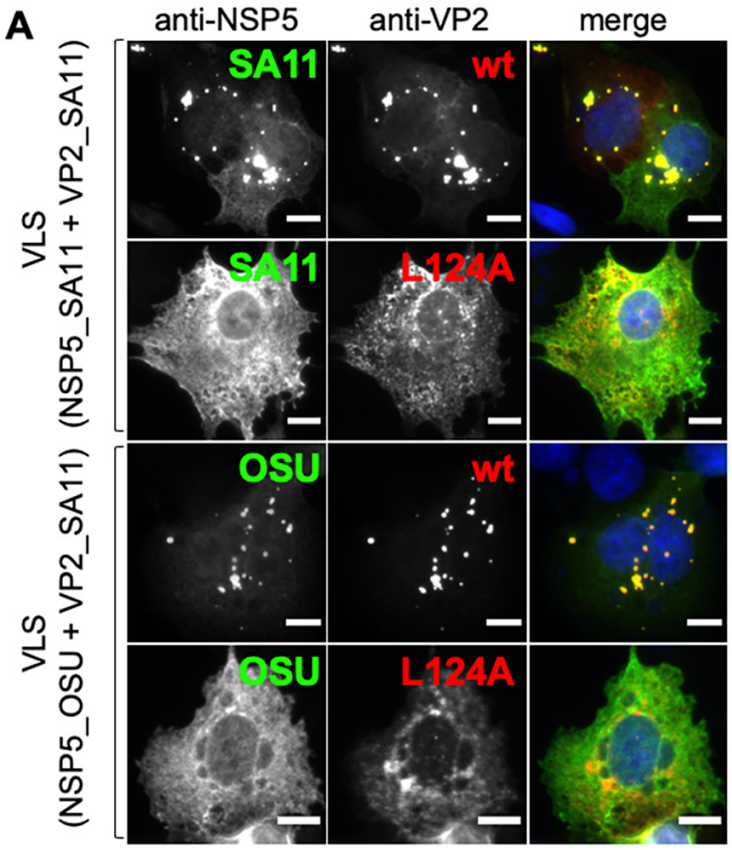

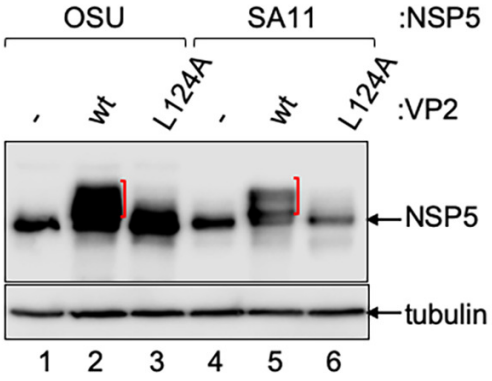

C

```
SA11    1   MSLSIDVTSLPSIPSTIYKNESSSTTSTLSGKSIGRSEQYISPDAEAFNKYMLSKSPEDI 60
            |||||||||||||:| | ||||||||||||||||||||||||||||||||||||||||||||
OSU     1   MSLSIDVTSLPSISSSIFKNESSSTTSTLSGKSIGRSEQYISPDAEAFNKYMLSKSPEDI 60

SA11    61  GPSDSASNDPLTSFSIRSNAVKTNADAGVSMDSSAQSRPSSNVGCDQVDFSLNKGLKVKA 120
            |||||||||||||||||||||||||||||| |||||||||||||||||:||::|:
OSU     61  GPSDSASNDPLTSFSIRSNAVKTNADAGVSMDSSTQSRPSSNVGCDQVDFSLTKGINVS- 119

SA11    121 NLDSSISISTDTKKEKSKQNHKSRKHYPRIEAESDSDDYVLDDSDSDDGKCKNCKYKKKY 180
            : ::| : : :::| ::: ::|||||||||||| |||:|||||||||||||||||||||||
OSU     120 ANLDSCVSISTDNKKEKSKKDKSRKHYPRIEADSDSEDYVLDDSDSDDGKCKNCKYKKKY 179

SA11    181 FALRMRMKQVAMQLIEDL 198
            ||||||||||||||||||
OSU     180 FALRMRMKQVAMQLIEDL 198
```